Progress In Electromagnetics Research M, Vol. 89, 111–120, 2020

Pattern Diversity MIMO 4G and 5G Wideband Circularly Polarized Antenna with Integrated LTE Band for Mobile Handset

Prashant Chaudhary[1], Ashwani Kumar[2, *], and Avanish Yadav[1]

Abstract—The present work describes a unique planar wideband circularly polarized MIMO antenna for 4G and Sub-6 5G band (1.35–2.75 GHz), with pattern diversity over the entire axial-ratio bandwidth. The design consists of two tri-branch planar inverted-F antenna (PIFA) antennas with a ground T-stub between the antennas, which is used to realize circular polarization and high isolation. The third antenna is an integrated Sub-6 5G (4.45–4.7 GHz) and LTE band (786.7–807.7 MHz) antenna, which is folded above the ground and placed vertically around the side. It also provides circular polarization at LTE band. The 3 dB axial ratio bandwidth (ARBW) of the MIMO antenna is 1.08 GHz (1.47–2.55 GHz); impedance matching bandwidth (IMBW) is 1.4 GHz (1.35–2.75 GHz); and its isolation is better than 13.4 dB in the whole band. It is fabricated on an FR-4 substrate and is suitable for mobile handset.

1. INTRODUCTION

In modern wireless communication systems, mobile phones are more and more important for us to communicate with others. Federal Communications Commission (FCC) calls mid-band of frequencies to Sub-6 band. Sub-6 GHz has advantages such as high transmission rate and short latency. Several countries specify the spectrum for Sub-6 GHz for 5G, which includes 2.5–2.6 GHz, 3.3–3.8 GHz, 4.5–5 GHz, and 3.8–4.2 GHz frequency bands [1]. Multiple-Input and Multiple-Output (MIMO) antennas operating either in Sub-6 GHz or antenna array in mm wave are used for receiving and sending many data signals instantaneously over the same radio channel [2–6]. MIMO system is very attractive for future 5G communication. Pattern diversity antennas are used to discriminate a large portion of the angular space. Circular polarization (CP) reduces both polarization loss and multipath interference, which is needed for high-speed data transmission and reception. In the past, several MIMO antennas were proposed for 5G application [2–6], 5G mobile MIMO antenna with null points of E-field to decouple the different inverted F antenna elements [2], 4-antenna MIMO system based on compact self-decoupled antenna pairs for 5G [3], dual-band MIMO antenna for 5G application [4], and Ground mode tuning (GMT) for the generation of CP [5]. 8-antenna MIMO system without any isolation elements or decoupling techniques were used [6], and a four-port MIMO antenna with a built-in circular-shaped isolator was proposed for Sub-6 GHz applications [7]. Two element broadband MIMO antenna with protrude and slot in the ground plane to reduce coupling is presented in [8]. CP MIMO antenna with both pattern and polarization diversity is designed in [9]. In [10], a MIMO antenna for metal frame design consists of six antenna in 2×2 array for LB LTE 4×4 array for H/MB configuration is presented. An ultrawide band MIMO antenna for mobile with high isolation is presented in [11] and consists of planar monopole with back to back tapered sots. Substrate integrated waveguide (SIW) is also used to generate CP reconfigurable antenna [12] while in [13] a cavity backed SIW antenna with a slot generates CP. Other designs are also reported for GNSS system and RFID system using CP antennas for reliable communication [14, 15]. The above-mentioned

Received 12 November 2019, Accepted 12 January 2020, Scheduled 31 January 2020
* Corresponding author: Ashwani Kumar (ashwanikumar7@yahoo.com).
[1] Department of Electronic Science, University of Delhi South Campus, New Delhi 110021, India. [2] Electronics and Communication Engineering, School of Engineering, Jawaharlal Nehru University, New Delhi 110067, India.

Sub-6 MIMO antennas have no circular polarization, and there is no integrated LTE band and 4G band, which are useful for LTE (800 MHz), 3G, 4G, as well as 5G.

In this work, we design a pattern diversity wideband CP MIMO antenna for 4G and 5G with integrated Sub-6 5G and LTE bands. The tri-branch planar inverted-F antennas (PIFAs) are separated with a ground T-stub, which is used to generate CP and high isolation; however, the third antenna is in 3D configuration, which is folded around the ground plane edges. and behaves as a multiband antenna. The final antenna covers the band of frequencies for LTE (800 MHz) 786.67–807.67 MHz, 1.35–2.75 GHz, (3G and 4G), 2.64–2.75 GHz, and 4.45–4.7 GHz (5G), respectively.

2. ANTENNA DESIGN

The layout and fabricated prototype of the proposed MIMO antenna is shown in Fig. 1. The antenna is designed on a 0.8 mm thick FR-4 substrate with permittivity of 4.4 and loss tangent of 0.02. The overall dimension is $120 \times 65 \times 4.8\,\text{mm}^3$ with a square ground of size $38 \times 38\,\text{mm}^2$. The proposed MIMO antenna structure consists of three PIFA antennas connected with a square ground plane. Two of them are tri-branch PIFAs, which are placed adjacent to the ground plane facing each other, and the third one is a vertical PIFA, which is bent around the adjacent edges of the ground plane with a uniform width of 1 mm. All the antennas are excited by a coaxial connector. The inner conductor of the coaxial is connected to the PIFAs, while the outer surface is fully connected to the ground. The dimensions of the antennas are as: $Ls = 120\,\text{mm}$, $Ws = 65\,\text{mm}$, $t = 4.2\,\text{mm}$, $t_1 = 1\,\text{mm}$, $L_1 = L_2 = 35\,\text{mm}$, $L_3 = 28\,\text{mm}$, $L_4 = 12\,\text{mm}$, $L_5 = 5\,\text{mm}$, $L_6 = 16.3\,\text{mm}$, $L_7 = 20.2\,\text{mm}$, $L_8 = 4\,\text{mm}$, $L_9 = 2\,\text{mm}$, $L_{10} = 4.3\,\text{mm}$, $L_{11} = 4.6\,\text{mm}$, $L_{12} = 13.3\,\text{mm}$, $L_{13} = 26.10\,\text{mm}$, $W = 38\,\text{mm}$, $W_1 = 0.8\,\text{mm}$, $W_2 = 1\,\text{mm}$, $W_3 = 1.7\,\text{mm}$, $W_4 = W_5 = 3\,\text{mm}$. The designed structure is simulated in Ansys HFSS.

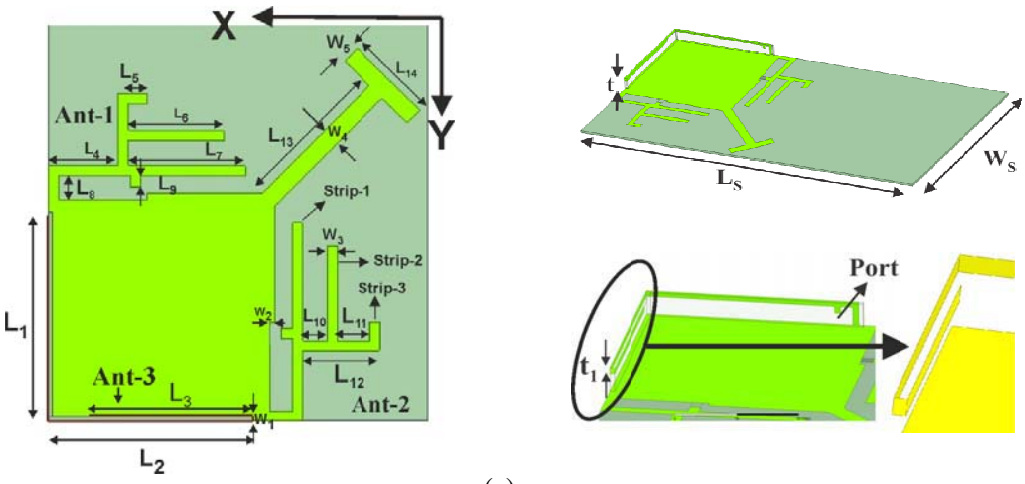

(a)

(b)

Figure 1. (a) Proposed antenna geometry. (b) Fabricated antenna with and without battery.

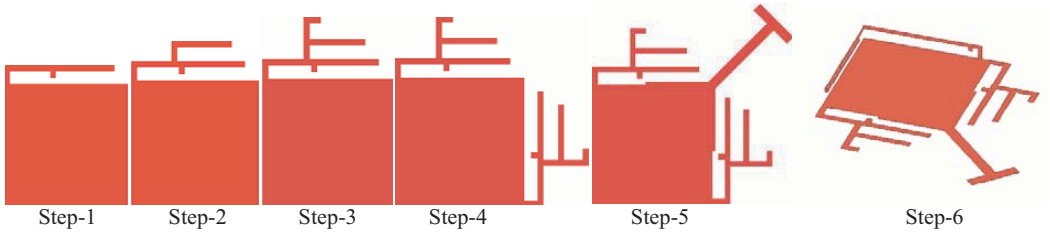

Figure 2. Design steps of the proposed antenna.

The proposed antenna has been designed in six sequential steps as illustrated in Fig. 2. Step-1 is a single inverted F-antenna while in step-2 one more strip is added to step-1 antenna. Similarly, in step-3 one more strip is added to step-2 antenna. The length of the step-1 antenna is $\frac{\lambda_g}{2} = 21\,\text{mm}$ (at $fc = 2.4\,\text{GHz}$), where $\lambda_g = \frac{\lambda_0}{\sqrt{\varepsilon_r}}$. Strip-2 and strip-3 are added to widen the impedance matching bandwidth. Fig. 3(a) shows the effect of each strip on the impedance matching bandwidth.

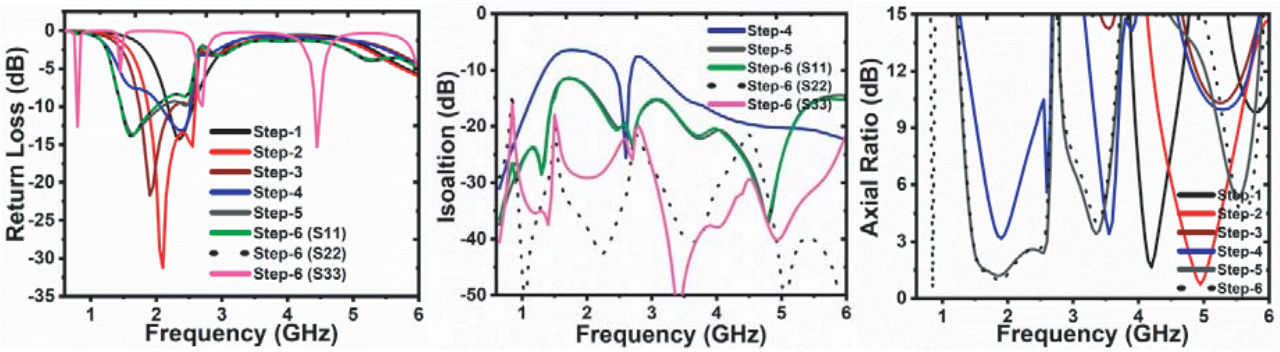

Figure 3. (a) Return loss. (b) Isolation. (c) Axial ratio of various design steps.

Now, in step-4 a similar second antenna (antenna-2) like in step-3 is placed adjacent to the ground plane to get a MIMO antenna. Since these antennas are very close, to avoid mutual coupling between them, a T-shaped stub is inserted in the ground plane between these antennas, which is step-5. These two antennas work for 3G and 4G bands, while for low frequency band LTE 800, a third antenna folded around the edges of ground plane is designed, which we called as step-6. Antenna-3 works as a multiband antenna. The size of this antenna can be obtained by using its lowest resonating frequency which is 800 MHz. The size of the third antenna is $\frac{\lambda_0}{4} = 99\,\text{mm}$ (at $fc = 800\,\text{MHz}$), $\lambda_0 = \frac{c}{fc}$ where c is the velocity of light.

Step-1 is a simple linearly polarized narrow band inverted-F antenna having 0.71 GHz (2.04–2.75 GHz), 6 dB impedance matching bandwidth (IMBW), as shown in Fig. 3(a), and out of band axial ratio bandwidth is 0.17 GHz at centre frequency 4.2 GHz, as shown in Fig. 3(c). In step-2, one inverted L-shaped strip is added, which behaves as an inductive loading and generating additional mode, which improves IMBW from 0.71 GHz (2.04–2.75 GHz) to 0.86 GHz (1.7–2.63 GHz), and out of band ARBW is also increased to 0.43 GHz. To further improve IMBW, another strip is added to step-2, which generates other additional modes. Now the IMBW is improved from 0.86 GHz to 0.96 GHz and the axial ratio increased above 10 dB all over the band as can be seen in Fig. 3(c). In step-4, a similar second antenna is placed adjacent to the ground plane, and the two antennas jointly work as a MIMO antenna. This combination or MIMO antenna further improves IMBW, which is now 1.10 GHz (1.48–2.48 GHz) while its axial ratio just touches 3 dB at 1.8 and 3.5 GHz. Since these antennas are very close, the isolation is below 6 dB, which is poor. To improve isolation, a T-shaped stub is inserted between the antennas, which will enhance the isolation more than 12 dB. A T-shaped stub improves both impedance

matching bandwidth and axial ratio bandwidth. The axial ratio bandwidth is 1.08 GHz (1.47–2.55 GHz), while impedance matching bandwidth is 1.4 GHz (1.35–2.75 GHz). The IMBW and ARBW can be seen in Fig. 3(a) and Fig. 3(c). The above designed antenna works in 1.35–2.75 GHz band. To add an additional band of LTE 800 and Sub-6 GHz, a folded inverted-F antenna-3 around the ground plane has been placed, which is a multiband antenna and can be seen in Fig. 2, which is a step-6. Performances of the antenna with different design steps are illustrated in Fig. 3 and in Table 1. Inverted-F antenna-3 has length nearly a quarter wavelength of $0.264\lambda_o$ (at $fc = 800$ MHz). The proposed antenna has IMBW 1.4 GHz (1.35–2.75 GHz); however, it has ARBW 1.08 GHz (1.47–2.55 GHz), as shown in Fig. 3(a) and Fig. 3(c). Fig. 3(b) shows the isolation, and it is improved by placing a T-shaped stub between two antennas.

Table 1. Performance of the antenna with different design steps.

Step	f_1, f_2 (GHz)	f_c (GHz)	Bandwidth	
			%	$f_2 - f_1$, GHz
1	2.04, 2.75	2.395	29.64	0.71
2	1.7, 2.63	2.165	39.72	0.86
3	1.64, 2.6	2.12	45.28	0.96
4	1.48, 2.48	1.98	55.55	1.10
5	1.35, 2.75	2.05	59.51	1.22
6	1.35–2.75, 0.786–0.807, 2.64–2.75, 4.45–4.7	2.05, 0.796, 2.695, 4.575	67.6, 2.63, 4.08, 5.46	1.4, 0.021, 0.11, 0.25

3. PARAMETRIC ANALYSIS

Some of the key parameters of the antenna have significant impact on the antenna performance. To understand the effect of these important key parameters, a parametric study is performed. To design an antenna with good performances, it is necessary to optimize the antenna's various parameters. These parameters are: Length of strip-1 (L_7), length of strip-2 (L_6), and length of strip-3 (L_5).

3.1. Effect of Strip-1 Length (L_7)

Length of strip-1 (L_7) has a major effect on performances of antenna-1 and antenna-2. IMBWs of antenna-1 and antenna-2 start improving with the length of strip-1, while there is an insignificant effect on the IMBW of antenna-3. As length of strip-1 increases, the IMBW improves from 0.96 GHz to 1.4 GHz up to $L_7 = 33.9$ mm. Further, increasing strip-1 length (L_7), the IMBW decreases; however, its ARBW starts appearing at 0.80 GHz as shown in Fig. 4.

Initially, when $L_7 = 17$ mm, a small dip of axial ratio appears at 5.5 GHz, and as L_7 increases further, the axial ratio is shifted toward the lower frequency side, which can be seen in Fig. 4(c). After After strip-1 length $L_7 = 27$ mm, the ARBW starts improving and becomes wide which is 0.82 GHz. The improved ARBW is observed for $L_7 = 33.9$ mm within the desired frequency band. Thus, optimized strip-1 length $L_7 = 33.9$ mm is chosen for the rest of the parametric study.

3.2. Effect of Strip-2 Length (L_6)

The effect of strip-2 length is presented in Fig. 5, and there is a need of optimization of this length to achieve the best performance. The IMBW for L_6 from 5 mm to 15 mm is nearly the same at 0.83 GHz, and hence it has insignificant effect up to 15 mm. Further increase in L_6 (up to 18 mm) provides improved IMBW to 1.4 GHz, and after $L_6 = 18$ mm, the IMBW again starts deteriorating to 0.85 GHz, as shown in Fig. 5(a). There is insignificant effect on IMBW of antenna-3 with strip-2 length. The ARBW is nearly the same around 1.08 GHz up to 18 mm and decreases with increase in L_6 as shown in

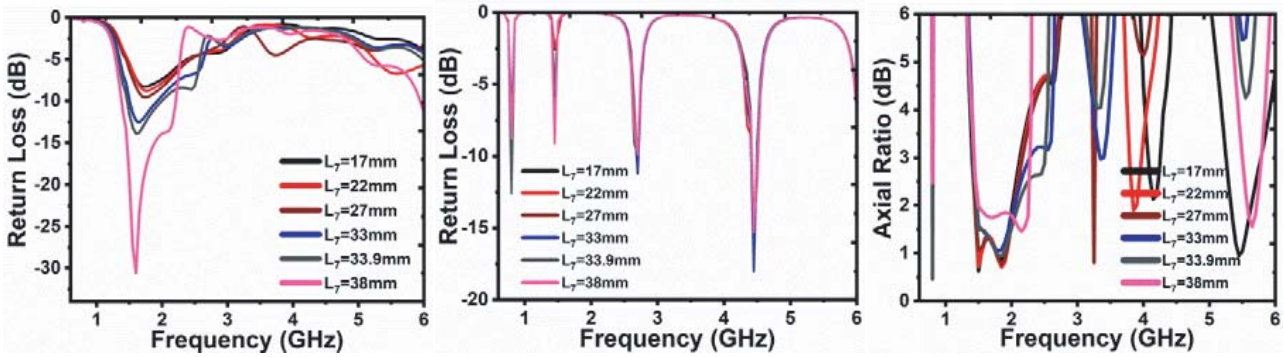

(a) (b) (c)

Figure 4. (a) Return loss of antenna-1/antenna-2. (b) Return loss of antenna-3. (c) Axial ratio of antenna-1/antenna-2/antenna-3 with length (L_7).

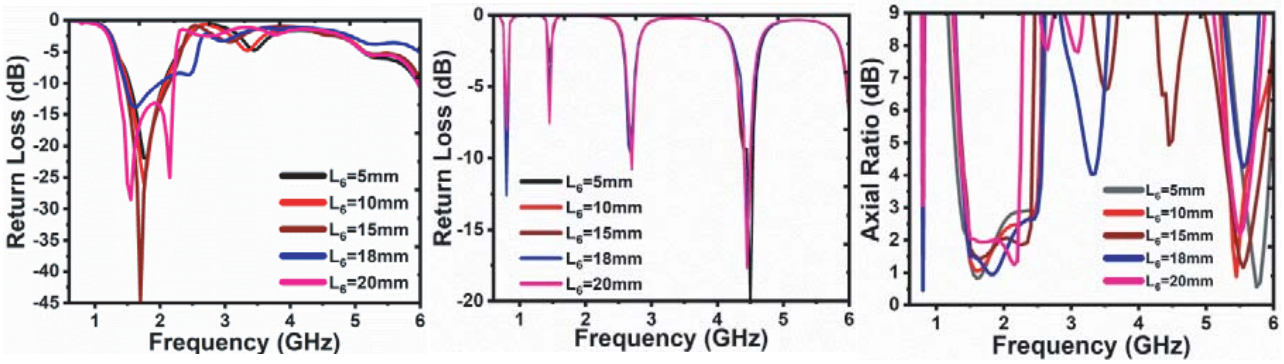

(a) (b) (c)

Figure 5. (a) Return loss of antenna-1/antenna-2. (b) Return loss of antenna-3. (c) Axial ratio of antenna-1/antenna-2/antenna-3 with length (L_6).

Fig. 5(c). There is no effect on the performance of antenna-3 as can be seen in Fig. 5(c). The optimized length of strip-2 is selected, $L_6 = 18$ mm, for the best performance of the designed antenna.

3.3. Effect of Strip-3 Length (L_5)

For fixed $L_7 = 33.9$ mm and $L_6 = 18$ mm, the effect of strip-3 length is presented in Fig. 6. The variation in IMBW of antenna-1 and antenna-2 is minor with L_5 as shown in Fig. 6(a). Its 6 dB IMBW is around 1.4 GHz while its ARBW is 1.08 GHz. Axial ratio dip at 800 MHz is decreased slightly to 3.6 dB at $L_5 = 6$ mm. For antenna-3, again there is an insignificant effect of L_5 on the IMBW and ARBW. The chosen value of L_5 is 5 mm.

4. *S*-PARAMETER, AXIAL RATIO AND PEAK GAIN

The simulated and measured return losses of the proposed antenna are shown in Fig. 7. Since antenna-1 and antenna-2 have the same dimensions, S_{11} and S_{22} are same, while antenna-3 works as a multiband antenna, and its return loss is presented with S_{33}. The mutual coupling between antenna-1 and antenna-2 can be reduced by placing the T-stub between the antennas. Ground T-stub not only improves the isolation but also generates the wideband CP. The impedance matching and axial ratio are mainly dependent on the T-stub. S_{11} and S_{22} of antenna-1 and antenna-2 cover the frequencies from 1.35 to 2.75 GHz, and the two antennas have the same impedance matching bandwidth which is 1.4 GHz. Antenna-3 shows tri-band behaviour, and it works for frequencies: 786.67–807.67 MHz, 2.64–2.75 GHz,

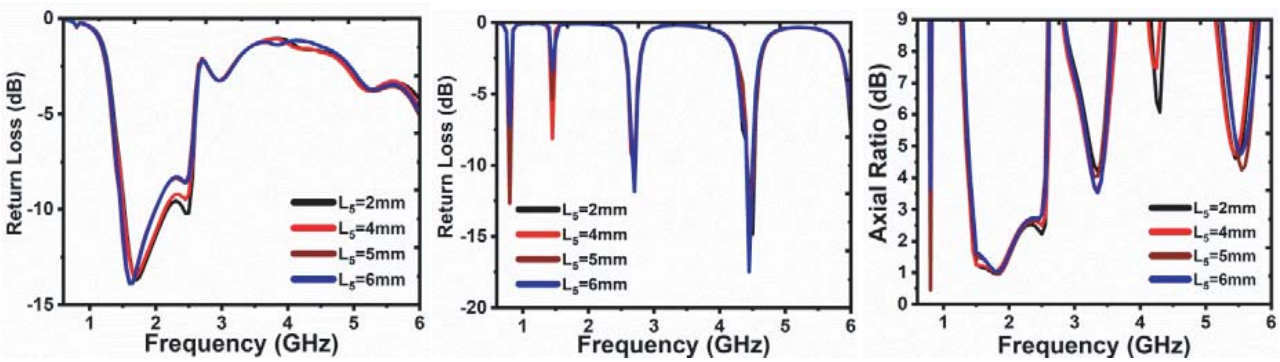

(a) (b) (c)

Figure 6. (a) Return loss of antenna-1/antenna-2. (b) Return loss of antenna-3. (c) Axial ratio of antenna-1/antenna-2/antenna-3 with length (L_5).

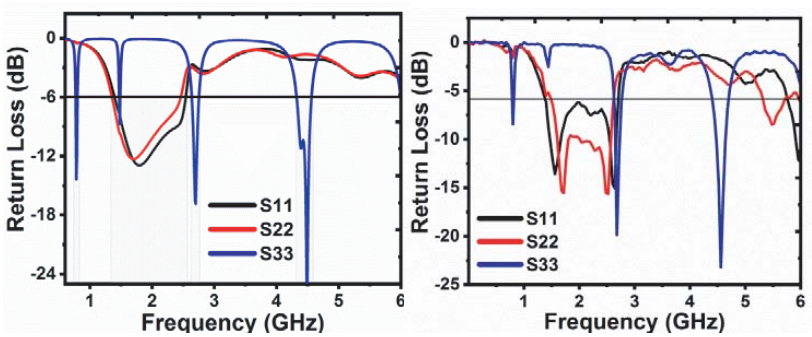

(a) (b)

Figure 7. Return Loss. (a) Simulated. (b) Measured.

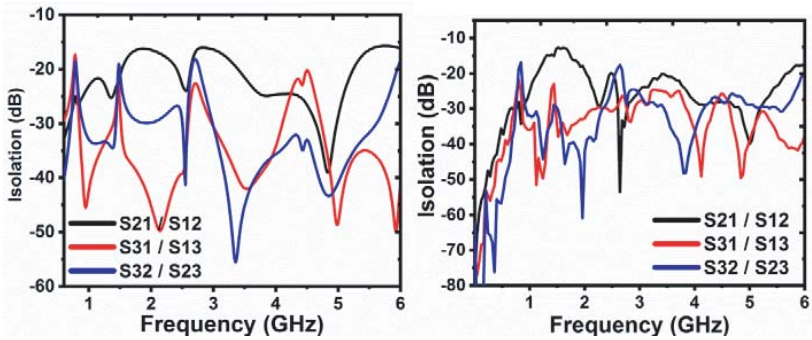

(a) (b)

Figure 8. Isolation. (a) Simulated. (b) Measured.

and 4.45–4.7 GHz as shown in Fig. 7(a). The measured results are very close to the simulated ones and are shown in Fig. 7(b). There is an insignificant effect of battery on both impedances matching and axial ratio characteristics. The proposed antenna with and without battery is shown in Fig. 1(b). The simulated isolations of all the antennas are better than −15 dB, while the measured isolation among all these three antennas are better than −13.4 dB, and it even improves at higher frequency, which can be seen in Fig. 8. The isolation between antenna-1 and antenna-2 is below −13.4 dB within the operating band. At 800 MHz, the isolation between antenna-3 and antenna-1/antenna-2 is below −15 dB.

The operation of antenna-3, which is multiband, can be further studied using surface current distribution at the three resonant frequencies. Fig. 7 shows the simulated and measured results. For

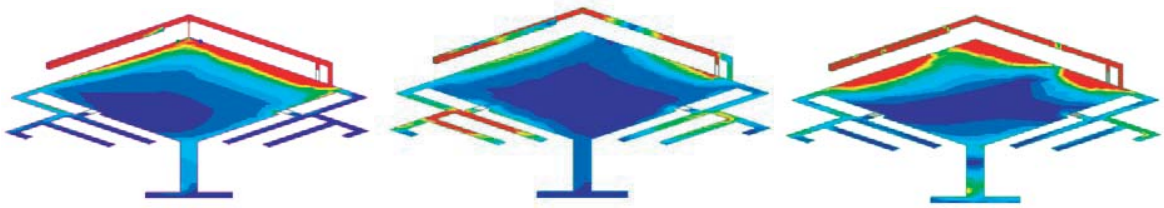

(a) (b) (c)

Figure 9. Surface current distribution at three different frequencies. (a) 800 MHz. (b) 2.6 GHz. (c) 4.6 GHz.

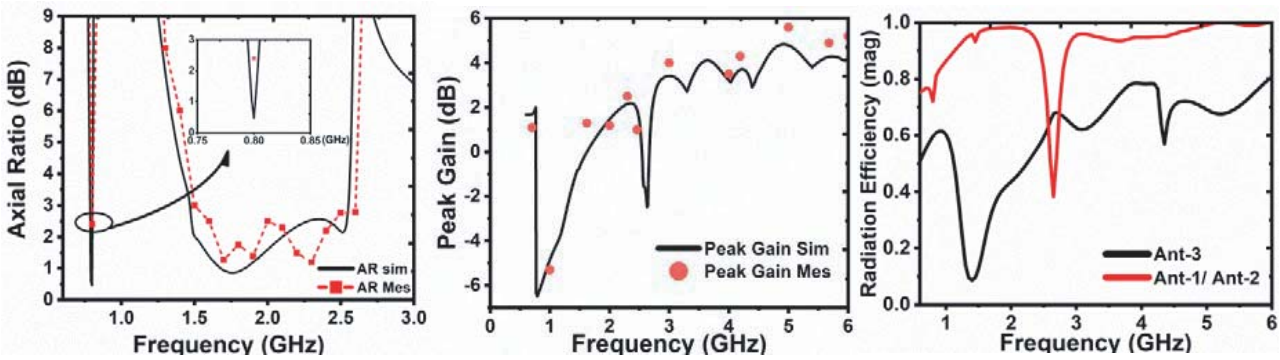

(a) (b) (c)

Figure 10. Measured and simulated. (a) Axial ratio. (b) Peak gain. (c) Simulated efficiency.

band-1 at 800 MHz, the current mainly flows on the surface of antenna-3, and this contributes most of the radiation shown in Fig. 9(a). Fig. 9(b) shows that the current concentrates at frequency 2.6 GHz mainly on the surface of antenna-3 and antenna-1, and this contributes the radiation for frequency 2.6 GHz. For band-3 at 4.6 GHz, Fig. 9(c) shows that the current mainly concentrates on antenna-3 and on the ground plane, which contributes in the radiation at frequency 4.6 GHz.

The simulated and measured axial ratios are shown in Fig. 10(a). The axial ratio is measured by employing a rotating linear method. This method employs a linearly polarized horn as a transmitting antenna with rotation, and our proposed antenna is used as a receiving antenna with fixed position. At the time of measurement, one antenna is connected with the vector network analyzer (VNA) while the other two are connected with the matched load. Our proposed MIMO antenna covers LTE band (786.71 to 807 MHz) and 1.35–2.75 GHz. The simulated lowest AR dip at boresight for antenna-3 is at 800 MHz, which is 0.56 dB, while in measurement it is 2.4 dB, and for antenna-1 and 2 it is from 1.5 GHz to 2.48 GHz. Peak gain at 800 MHz is 1.5 dB, while it varies from 1.5 dB to 3.7 dB for frequencies 1.35–2.75 GHz and 4.45–4.7 GHz, respectively. The simulated and measured gains are shown in Fig. 10(b). The simulated efficiency of the proposed antenna-1/antenna-2 is presented in Fig. 10(c), which is more than 85% in all the frequency bands, and for antenna-3 it varies from 50% to 78% in the multiband frequency.

5. MIMO PERFORMANCE

Envelop correlation coefficient (ECC) and diversity gain (DG) are two important parameters in MIMO antenna. In MIMO each antenna is near another antenna, hence chance of coupling is very high. The ECC factor gives how much their radiation patterns are spatially apart in space. It is also important to achieve feasible diversity gain. The lower the correlation factor is, the higher the diversity gain is. Correlation factor between antenna-1 and antenna-2 is less than 0.026 over the band 1.35–2.75 GHz shown in Fig. 11(a), whereas the correlation between antenna-1 and antenna-3 is less than 0.3 all over the four frequency bands, which are centred at 800 MHz, 1.975 GHz, 2.695 GHz, and 4.57 GHz. Correlation

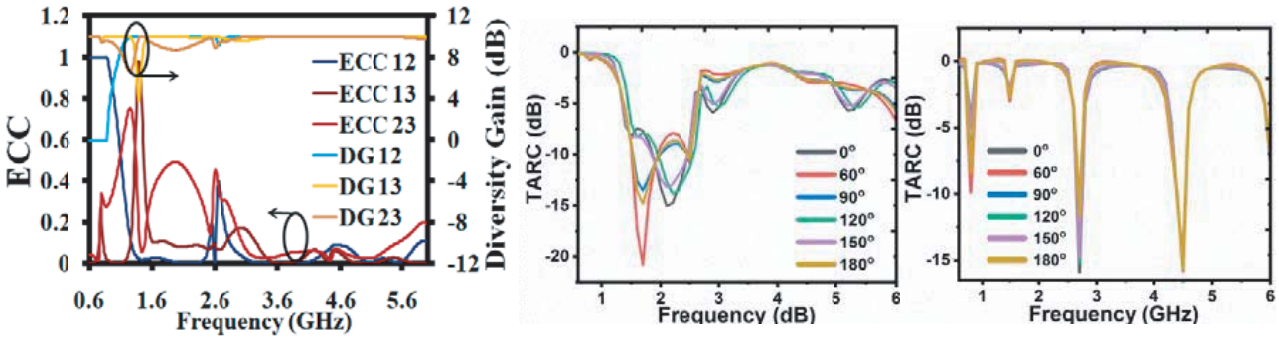

(a) (b) (c)

Figure 11. (a) ECC and DG. (b) TARC between antenna-1 and antenna-2. (c) TARC between antenna-3 and antenna-1/antenna-2.

factor between antenna-2 and antenna-3 is also below 0.43 at 2.695 GHz, and in other frequencies it is very low. The multiple channels increase the link capacity, which improves reliability of the system, measured in terms of diversity gain. DGs of all antennas are between 9.2 and 10 dB all over the bands of frequencies as shown in Fig. 11(a). The total active reflection coefficient (TARC) is referred to as square of the ratio of reflected power to the incident power for a MIMO antenna system. The TARC between antenna-1 and antenna-2, antenna-1 and antenna-3 and antenna-2 and antenna-3 is best for the 0° phase difference and it is worst for 180° phase difference. The TARC between antenna-1 and antenna-2 below −7.5 dB coveres the whole band from 1.35 to 2.75 GHz and also at 800 MHz shown in Fig. 11(b). The TARC between antenna-3 and antenna-1/antenna-2 is also below −7.5 dB in the whole working band shown in Fig. 11(c). Our proposed antenna is compared in Table 2 with the earlier published works, which shows that its performance is comparable.

Table 2. Performance comparison with recently published work.

Ref.	LTEFreq., BW (MHz)	3G, 4G, 5 GHz, BW	5G Sub-6, Freq., BW (GHz)	Axial Ratio, BW (GHz)	Gain (dBi)	Size (mm × mm × mm)
2	-	-	(3.4–3.6) 20 MHz	-	2.7–3.9	100 × 50
3	-	-	(3.4–3.6) 20 MHz	-	3	150 × 75 × 0.8
4	-	2.36–2.53, 0.17		2.38–2.52, 0.14	0.15–0.77	110 × 55 × 0.5
5	-	-	(3.4–3.6) 20 MHz	-	−2	30 × 30 × 1
6	-	-	(3.6–4) 2 GHz	-	3.6–4.0	150 × 75 × 0.8
Our	**786.7–807.7, 21**	**0.02 (1.43–1.47), 0.11 (2.64–2.75), 1.4 (1.35–2.75)**	**2.3 GHz and 2.5/2.6, 4.45–4.7**	**20.3 MHz (786.7–807), 1.08 GHz (1.47–2.55)**	**1.5–3.5**	120 × 65 × 4.8

6. RADIATION PATTERN

From the radiation pattern in X-Y plane for antenna-1, the maximum radiation pattern is directed toward 60°, and for antenna-2 it is directed along 150° showing pattern diversity as shown in Fig. 12 at

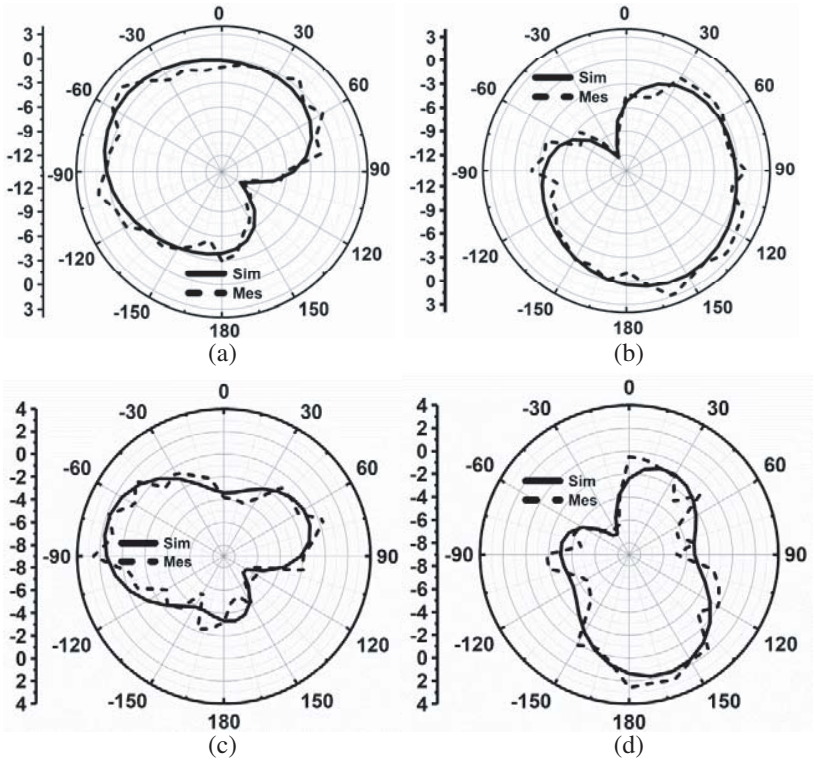

Figure 12. Radiation pattern in XY plane at 1.7 GHz. (a) Port-1. (b) Port-2 and at 2.1 GHz. (c) Port-1. (d) Port-2.

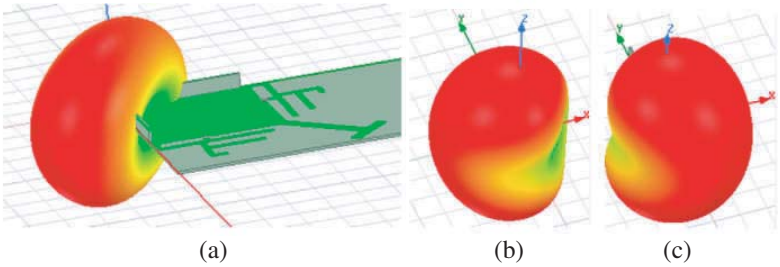

Figure 13. 3D radiation pattern. (a) Antenna-3. (b) Antenna-1. (c) Antenna-2.

1.7 GHz and 2.1 GHz. Antenna radiation patterns are distinctly directed outside, hence radiating most of the power outside the handset, which will reduce the effect of the radiation on the head. Fig. 13(a) shows the 3D radiation pattern of antenna-3 while Figs. 13(b)–(c) show the 3D radiation patterns of antenna-1 and antenna-2 at 1.7 GHz.

7. CONCLUSION

The design of a wideband circularly polarized integrated LTE 800MIMO antenna with 4G having pattern diversity and Sub-6 5G band is presented in this paper. The designed antenna can be easily integrated in a mobile phone, and its performances are measured with and without using battery. The proposed antenna radiates most of its radiation outside. Antenna-1 and antenna-2 radiation patterns are directional whereas antenna-3 radiation pattern is omnidirectional, which provides better coverage. The proposed antenna could be useful for a mobile handset.

REFERENCES

1. 5G Spectrum, "GSMA public policy position," *GSMA Latin America*, Jul. 2019.
2. Zhao, X., S. P. Yeo, and L. C. Ong, "Decoupling of inverted-F antennas with high-order modes of ground plane for 5G mobile MIMO platform," *IEEE Trans. on Antennas Prop.*, Vol. 66, No. 9, 4485–4495, 2018.
3. Ren, Z., A. Zhao, and S. Wu, "MIMO antenna with compact decoupled antenna pairs for 5G mobile terminals," *IEEE Antennas Wireless Prop. Lett.*, Vol. 18, No. 7, 1367–1371, 2019.
4. Marzouk, H. M., M. I. Ahmed, and A.-E. H. Shaalan, "Novel dual-band 28/38 GHz MIMO antennas for 5G mobile applications," *Progress In Electromagnetics Research C*, Vol. 93, 103–117, 2019.
5. Qu, L., Z. Zahid, H. H. Kim, and H. Kim, "Circular polarized ground radiation antenna for mobile applications," *IEEE Trans. on Antennas Prop.*, Vol. 66, No. 5, 2655–2660, 2018.
6. Zhao, A. and Z. Ren, "Size reduction of self-isolated MIMO antenna system for 5G mobile phone applications," *IEEE Antennas Wireless Prop. Lett.*, Vol. 1, No. 19, 152–156, 2018.
7. Saxena, S., B. K. Kanaujia, S. Dwari, S. Kumar, and R. Tiwari, "MIMO antenna with built-in circular shaped isolator for Sub-6 GHz 5G applications," *Electron. Lett.*, Vol. 54, No. 8, 478–480, 2018.
8. Xia, X.-X., Q.-X. Chu, and J.-F. Li, "Design of a compact wideband MIMO antenna for mobile terminals," *Progress In Electromagnetics Research C*, Vol. 41, 163–174, 2013.
9. Chaudhary, P., A. Kumar, and B. K. Kanaujia, "A low-profile wideband circularly polarized MIMO antenna with pattern and polarization diversity," *International Journal of Microwave and Wireless Technologies*, 1–7, 2019.
10. Barani, I. R. R. and K. L. Wong, "Integrated inverted-F and open-slot antennas in the metal-framed smartphone for 2×2 LTE L band 4×4 LTE M/HB MIMO operations," *IEEE Trans. on Antennas Prop.*, Vol. 66, No. 10, 5004–5012, 2018.
11. Nie, L. Y., X. Q. Lin, Z. Q. Yang, J. Zhang, and B. Wang, "Structure-shared planar UWB MIMO antenna with high isolation for mobile platform," *IEEE Trans. on Antennas Prop.*, Vol. 67, No. 34, 2735–2738, 2018.
12. Hao, Z. C., K. Fan, and H. Wang, "A planar polarization-reconfigurable antenna," *IEEE Trans. on Antennas Prop.*, Vol. 65, No. 4, 1624–1632, 2017.
13. Kumar, A., D. Chaturvedi, and S. Raghavan, "SIW cavity-backed circularly polarized square ring slot antenna with wide axial-ratio bandwidth," *International Journal of Electronics and Communications*, Vol. 94, 122–127, 2018.
14. Tran, H. H., S. X. Ta, and I. Park, "Single-feed, wideband, circularly polarized, crossed bowtie dipole antenna for global navigation satellite systems," *J. Electromagnetics Eng. Sci.*, Vol. 14, No. 3, 299–305, Sep. 2014.
15. Lu, Y.-L., H.-R. Cui, X.-W. Sun, M. Xu, and Y.-Z. Yin, "A simple UHF RFID circularly-polarized reader antenna design," *Proc. Electr. Design Adv. Packag. Syst. Symp. (EDAPS)*, 1–2, Hangzhou, China, Dec. 2011.